AMERICAN SOCIETY FOR MICROBIOLOGY | Applied and Environmental Microbiology

Spotlight Selection | Structural Biology | Full-Length Text

The unique salt bridge network in GlacPETase: a key to its stability

Xiaoyan Qi,[1] Yanfei Wu,[1] Shu-Ting Zhang,[1] Chao-Fan Yin,[1] Mukan Ji,[2] Yongqin Liu,[2] Ying Xu,[1] Ning-Yi Zhou[1]

AUTHOR AFFILIATIONS See affiliation list on p. 13.

ABSTRACT The extensive accumulation of polyethylene terephthalate (PET) has become a critical environmental issue. PET hydrolases can break down PET into its building blocks. Recently, we identified a glacial PET hydrolase GlacPETase sharing less than 31% amino acid identity with any known PET hydrolases. In this study, the crystal structure of GlacPETase was determined at 1.8 Å resolution, revealing unique structural features including a distinctive N-terminal disulfide bond and a specific salt bridge network. Site-directed mutagenesis demonstrated that the disruption of the N-terminal disulfide bond did not reduce GlacPETase's thermostability or its catalytic activity on PET. However, mutations in the salt bridges resulted in changes in melting temperature ranging from −8°C to +2°C and the activity on PET ranging from 17.5% to 145.5% compared to the wild type. Molecular dynamics simulations revealed that these salt bridges stabilized the GlacPETase's structure by maintaining their surrounding structure. Phylogenetic analysis indicated that GlacPETase represented a distinct branch within PET hydrolases-like proteins, with the salt bridges and disulfide bonds in this branch being relatively conserved. This research contributed to the improvement of our comprehension of the structural mechanisms that dictate the thermostability of PET hydrolases, highlighting the diverse characteristics and adaptability observed within PET hydrolases.

IMPORTANCE The pervasive problem of polyethylene terephthalate (PET) pollution in various terrestrial and marine environments is widely acknowledged and continues to escalate. PET hydrolases, such as GlacPETase in this study, offered a solution for breaking down PET. Its unique origin and less than 31% identity with any known PET hydrolases have driven us to resolve its structure. Here, we report the correlation between its unique structure and biochemical properties, focusing on an N-terminal disulfide bond and specific salt bridges. Through site-directed mutagenesis experiments and molecular dynamics simulations, the roles of the N-terminal disulfide bond and salt bridges were elucidated in GlacPETase. This research enhanced our understanding of the role of salt bridges in the thermostability of PET hydrolases, providing a valuable reference for the future engineering of PET hydrolases.

KEYWORDS molecular dynamics, PET hydrolase, salt bridges, structure, thermostability

The advantageous properties of plastics, such as high moldability, lightweight, and low cost, have driven their prevalent incorporation into industrial manufacturing and daily life. However, current global plastic production exceeds 367 million tons annually (1), and only approximately 9% of them are recycled, while most plastics are discarded, landfilled, or incinerated (2). Discarded plastics can be further fragmented into microplastics through weathering processes and mechanical abrasion (3). Consequently, microplastic pollution has now become pervasive across marine and terrestrial ecosystems, posing ecological threats across multiple trophic levels (4). Polyethylene terephthalate (PET), ranking as the sixth most-produced plastic globally (5), is commonly

Editor Haruyuki Atomi, Kyoto University, Kyoto, Japan

Address correspondence to Ning-Yi Zhou, ningyi.zhou@sjtu.edu.cn.

The authors declare no conflict of interest.

See the funding table on p. 14.

Received 12 December 2023
Accepted 25 January 2024
Published 15 February 2024

[This article was published on 15 February 2024 with an incorrect accession number in the Data Availability statement. The number was updated in the current version, posted on 23 February 2024.]

used in various applications including bottles, films, and fibers. PET is an aromatic polyester synthesized by the condensation of terephthalic acid (TPA) and ethylene glycol (EG) monomers. The extensive production and consumption of PET have led to its massive accumulation in the environment, risking ecosystem, and human health (6).

PET hydrolases can depolymerize PET into its building blocks, providing a cost-effective and sustainable solution to PET pollution. In recent years, various sources of PET hydrolases have been identified and analyzed biochemically and structurally, including lipases, cutinases, carboxylesterases, and esterases (7). In 2016, Yoshida et al. identified a key PET-degrading enzyme, *Is*PETase, from a PET-assimilating bacterial strain *Ideonella sakaiensis* 201-F6 (8). This PET hydrolase was able to degrade PET at ambient temperatures (8). It featured two disulfide bonds, one at the C-terminus and the other one near the active site (9). Meanwhile, there is another class of thermophilic PET hydrolases including Cut190, TfCut2, and LCC with single disulfide bonds at the C-terminus (9), whose optimal reaction temperatures range from 50°C to 65°C (7). It is reported that as the temperature approached the glass transition temperature of PET, the polymer chains exhibited increased flexibility, consequently rendering them more susceptible to enzymatic attack (10). Therefore, various researchers have attempted to improve the PET hydrolysis efficiency of PET hydrolases by improving their thermostability. The adopted approach often incorporates the utilization of features relating to protein thermostability, such as disulfide bonds and salt bridges. For example, a disulfide bond was introduced into LCC to improve its thermal stability and performance for PET degradation (11). A pair of salt bridge from LCC was grafted into *Is*PETase to enhance its thermal stability and the activity on PET (12). This indicates that disulfide bonds and salt bridges are crucial for improving the thermostability of PET hydrolases. However, in the diverse PET hydrolases, the mechanisms of disulfide bonds and salt bridges influencing stability remain unexplored.

Recently, we identified a PET hydrolase GlacPETase from the glacier microbiome (13). It exhibited a comparable activity on PET with *Is*PETase at ambient temperatures and a better thermostability (13). GlacPETase shared less than 31% amino acid identity with any known PET hydrolases. From the predicted structure, it does not contain the conserved C-terminal disulfide bond like LCC or the conserved disulfide bond located near the catalytic center like *Is*PETase (13). Instead, it contains a unique disulfide bond at the N-terminus (13). These unique features of this glacial-derived enzyme render it an appealing candidate for further study.

In this study, the crystal structure of GlacPETase was determined, revealing its N-terminal disulfide bond and a unique salt bridge network. This work excavated the novel structural features of GlacPETase, not only advancing our fundamental understanding of the structural mechanisms governing the thermostability of PET hydrolases but also broadening our knowledge of the diversity and plasticity among PET hydrolases.

RESULTS

Overall structure and novel features of GlacPETase

The GlacPETase crystal structure was solved at 1.80 Å resolution and two chains were observed in an asymmetric unit (Fig. 1A). There was no significant difference in the structure of the two chains after structure alignment [root mean square deviation (RMSD) for Cα =0.215, Fig. 1B]. The diffraction data and refinement statistics are listed in Table S2. According to the structure, GlacPETase was a classical α/β hydrolase, arranged as β1-β2-β3-α1-β4-α2-β5-α3-β6-α4-β7-α5-β8-α6-α7-α8-α9-β9 (Fig. 1C). Similar to *Is*PETase (9), GlacPETase adopted catalytic triad composed of Ser147, His227, and Asp196 (Fig. 1D). Ser147 functioned as the nucleophile, positioned 2.8 Å away from the base His227 for polarization. Meanwhile, His227 was stabilized by the presence of the acid Asp196 with a distance of 2.7 Å (Fig. 1D).

Compared to its homologous enzymes, GlacPETase harbored some distinctive features in disulfide bond and salt bridges. Only one single intra-molecular disulfide bond was observed in GlacPETase (Fig. 1C and 2A). The disulfide bond was located at

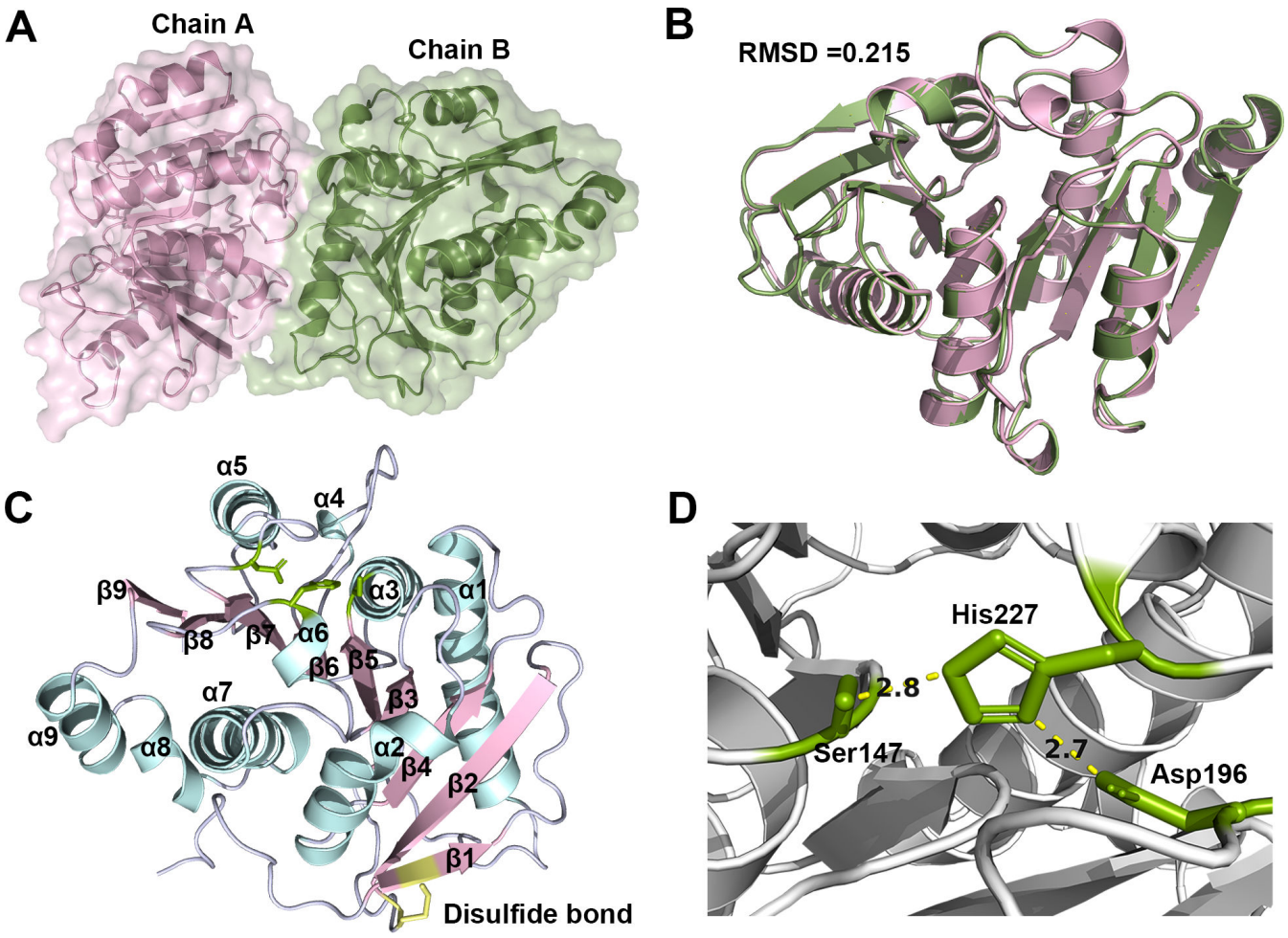

FIG 1 Overall structure of GlacPETase. (A) The two polypeptide chains in an asymmertric unit of GlacPETase. Chain A is colored pink and Chain B green. (B) The alignment of Chain A and Chain B with a root mean square deviation (RMSD) for Cα of 0.215 Å. (C) The overall structure of GlacPETase is shown as a cartoon model. The catalytic triad (green, top) and disulfide bond (yellow, bottom) are shown as sticks. (D) The catalytic triad is composed of Ser147, His227, and Asp196. Ser147 serves as the nucleophile and is located 2.8 Å away from the base His227. The acid Asp196 is located 2.7 Å away from His227 to provide stabilization.

the N-terminus of GlacPETase, connecting the first β-strand to the loop in front of the second β-strand (Fig. 1C). However, a class of its homologous PET hydrolases like LCC consistently exhibits a conserved disulfide bond at the C-terminus, linking the last helix to the loop in front of the last β-strand. Another class of homologous PET hydrolases like *Is*PETase features an extra disulfide bond linking two loops where the catalytic acid and base are situated (14). GlacPETase possessed 46 charged amino acids, with 17 of them involved in the formation of salt bridges (Table S3). The formation of these salt bridges is attributed to the proximity of the carboxyl groups of acidic residues and the amino groups of basic residues, with a distance within 4 Å (Fig. 3). The salt bridge network in GlacPETase differed significantly from that of its homologous enzymes (Table 1), which will be elaborated upon in the following sections.

N-terminal disulfide bond in GlacPETase: limited impact on its stability and PET catalytic activity

To assess the impact of the N-terminal disulfide bond on the structure and function of GlacPETase, two cysteine residues responsible for forming the disulfide bond were individually mutated to serine. Subsequently, the mutant proteins were purified and subjected to melting temperature (Tm) determination and assessment of PET hydrolysis

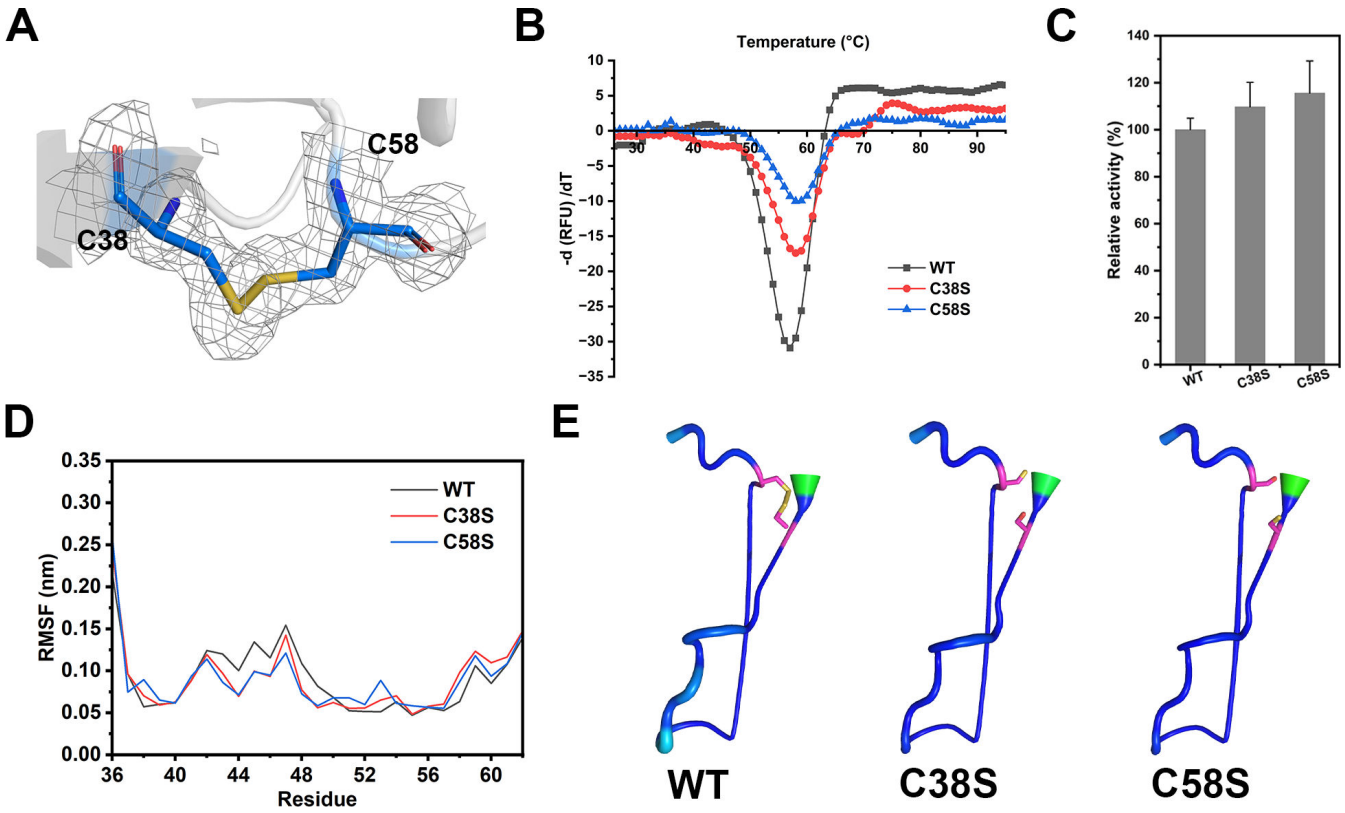

FIG 2 The N-terminal disulfide bond of GlacPETase and its functional validation. (A) The N-terminal disulfide bond of GlacPETase. The structure of the disulfide bond is depicted as a stick model and the omitted electron density map (gray mesh) of the residues involved in the disulfide bond is contoured at 2.0 *σ*. (B) The melting temperatures of GlacPETase and its mutants C38S and C58S. (C) The relative activities of GlacPETase and its mutants C38S and C58S. (D) The average root mean square fluctuation (RMSF) for Cα of residues 36–62 in the molecular dynamics simulation for WT and its mutants C38S and C58S. (E) Porcupine plot of residues 36–62 in the molecular dynamics simulation for WT and its mutants C38S and C58S. Cysteine involved in forming disulfide bonds, or serine after mutation, was represented using pink sticks. Regions with high fluctuations (high RMSF) were displayed in a thicker, teal color, while areas with low fluctuations (low RMSF) were shown in blue.

activity. The results indicated that the mutants, C38S and C58S, exhibited Tm values of 58°C, surpassing that of the wild type (56°C) by two degrees (Fig. 2B). Compared to the wild type, the mutants C38S and C58S exhibited an increased PET activity, reaching 109.7% and 115.6%, respectively (Fig. 2C). Subsequently, molecular dynamics simulations were performed on the wild type (WT) and its mutants C38S and C58S to further investigate the structural implications of the mutations. As shown in Fig. 2D, the serine mutations did not lead to significant fluctuations in the protein structure near where the disulfide bonds were located. The porcupine plot in Fig. 2E further visualized the RMSF for Cα of the structure formed by residues 36 to 62 during the molecular dynamics simulation. Little variations in the thickness and color of the lines suggested no significant impact on the structure of GlacPETase after serine mutation at the disulfide bond site. These findings implied that the N-terminal disulfide bond of GlacPETase was not actually playing an important role in maintaining the structure or its catalytic activity on PET.

GlacPETase possesses a unique salt bridge network

Analysis of salt bridges revealed the formation of nine pairs of salt bridges in GlacPETase (Table S3; Fig. 3). Among them, K115 formed salt bridges with both D159 and E111 (Fig. 3G). H227 and D196 were components of the catalytic triad, playing a crucial role in substrate catalysis. D196 stabilized H227 through salt bridge interactions (Fig. 3B). H227/D196, R238/D229, and R127/E124 displayed a ≤ 20% accessible surface area (ASA) and

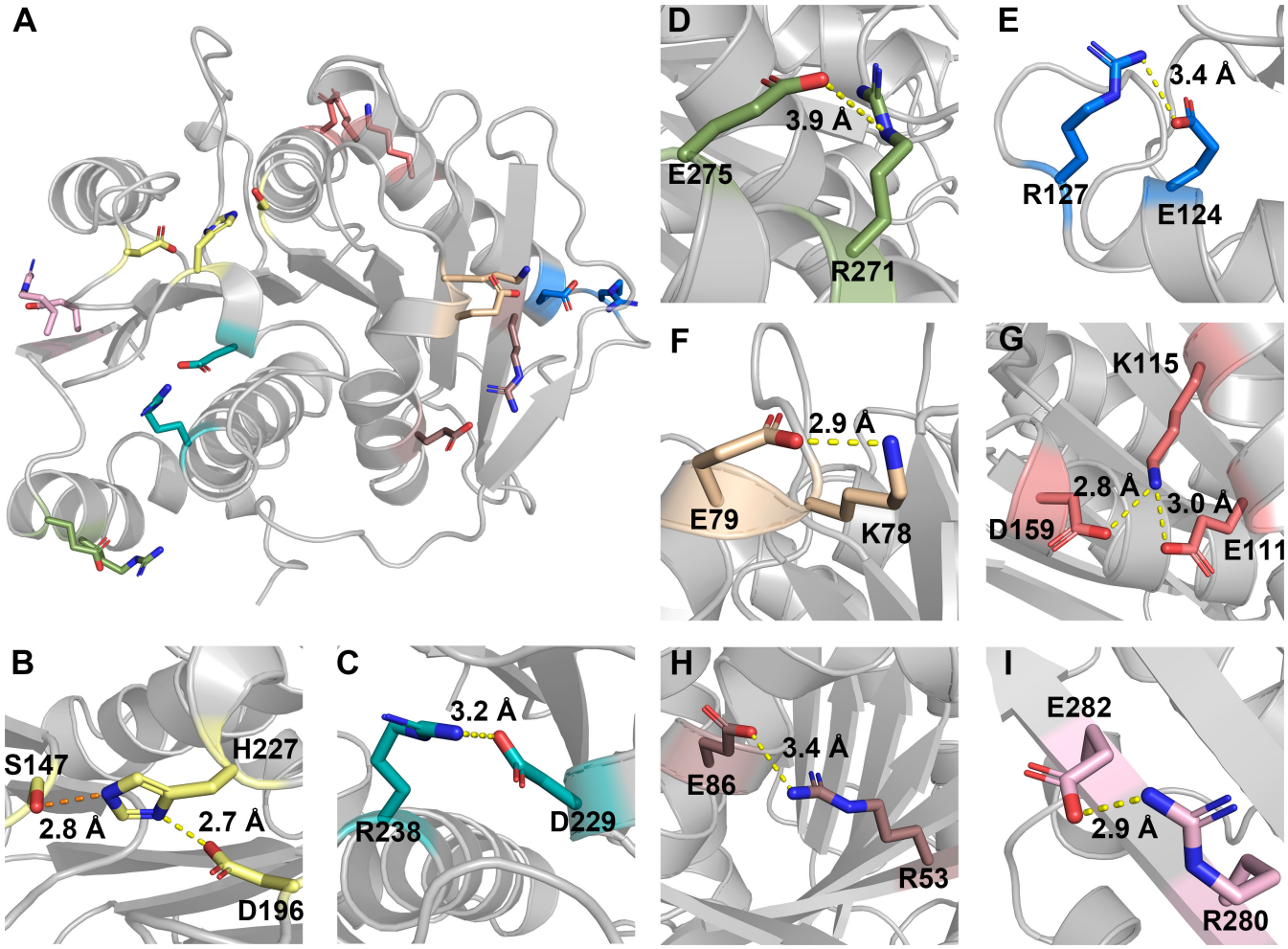

FIG 3 The salt bridge distribution of GlacPETase. (A) The nine pairs of salt bridges in GlacPETase. Each pair of salt bridges is marked with a different color. (B) The salt bridge connected by D196 and H227 was colored yellow with a distance of 2.7 Å. (C) The salt bridge connected by R238 and D229 was colored cyan with a distance of 3.2 Å. (D) The salt bridge connected by R271 and E275 was colored green with a distance of 3.9 Å. (E) The salt bridge connected by R127 and E124 was colored blue with a distance of 3.4 Å. (F) The salt bridge connected by K78 and E79 was colored gold with a distance of 2.9 Å. (G) The salt bridge connected by K115 and E111/D159 was colored magenta with a distance of 3.0 Å and 2.8 Å respectively. (H) The salt bridge connected by R53 and E86 was colored deep pink with a distance of 3.4 Å. (I) The salt bridge connected by R280 and E282 was colored light pink with a distance of 2.9 Å.

were then classified as buried. By contrast, R271/E275, K78/E79, K115/D159, K115/E111, R53/E86 and R280/E282 were exposed (≥ 20% ASA) (Table S3).

Multiple sequence alignment and structural alignment showed that GlacPETase possessed a unique salt bridge network compared to its homologous proteins (Table 1; Fig. S1). The salt bridge positions in Table 1 were ranked according to their occurrence frequency in various PET hydrolases. It can be observed that the salt bridge formed by D196 and H227 was strictly conserved across all PET hydrolases (SB 1, Table 1). The three salt bridges in LCC involving D155/R158, D267/R269, and D267/R158 were also strictly conserved in Cut190, TfCut_2, *Is*PETase, PE-H, and Ple629 but were absent only in GlacPETase (SB 2–4, Table 1). GlacPETase possessed as many as seven additional salt bridges that were not found in all other homologous proteins (SB 13–19, Table 1). By contrast, *Is*PETase contained six salt bridges but all of them can be found in other homologous proteins, lacking its signature salt bridges (SB 1–6, Table 1). These findings indicated that GlacPETase possessed a unique salt bridge network.

TABLE 1 The salt bridge distribution of several typical PET hydrolases[b]

Salt bridges[a]	GlacPETase	LCC	Cut190	TfCut_2	*Is*PETase	PE-H	Ple629
SB 1	D196/H227	D210/H242	D222/H254	D176/H208	D177/H208	D217/H249	D198/H230
SB 2	\	D155/R158	D166/R169	D120/R123	D121/R124	D161/R164	D142/R145
SB 3	\	D267/R269	D279/R281	D233/R235	D236/R238	D277/R279	D262/R263
SB 4	\	D267/R158	D277/R169	D231/R123	D234/R124	D275/R164	D260/R145
SB 5	R280/E282	R286/D284	E297/R299	\	D254/R256	D297/R299	D282/R284
SB 6	\	\	E61/K266	\	E15/K223	E54/R264	E35/R249
SB 7	\	\	D151/R189	\	\	D143/R185	D124/R166
SB 8	\	D129/H191	\	R178/H156	\	\	\
SB 9	\	D129/R173	\	D94/R138	\	\	\
SB 10	\	\	D54/R281	\	\	D47/R279	\
SB 11	\	\	K266/D292	\	\	\	D277/R249
SB 12	\	\	\	\	\	D196/R179	D177/R160
SB 13	R271/E275	\	\	\	\	\	\
SB 14	D229/R238	\	\	\	\	\	\
SB 15	E86/R53	\	\	\	\	\	\
SB 16	K78/E79	\	\	\	\	\	\
SB 17	K115/D159	\	\	\	\	\	\
SB 18	K115/E111	\	\	\	\	\	\
SB 19	E124/R127	\	\	\	\	\	\
SB 20	\	D53/R108	\	\	\	\	\
SB 21	\	D98/R124	\	\	\	\	\
SB 22	\	R173/D193	\	\	\	\	\
SB 23	\	R173/E176	\	\	\	\	\
SB 24	\	\	R159/E163	\	\	\	\
SB 25	\	\	E236/R299	\	\	\	\
SB 26	\	\	\	K216/E251	\	\	\
SB 27	\	\	\	K229/D12	\	\	\
SB 28	\	\	\	R143/D145	\	\	\
SB 29	\	\	\	\	\	D123/R66	\
SB 30	\	\	\	\	\	D238/H273	\
SB 31	\	\	\	\	\	\	D208/R284

[a]The order of salt bridges (SB) naming is based on their occurrence frequency in various PET hydrolases, from high to low.
[b]The slash (\) means that the salt bridge at this location is absent in this PET hydrolase.

Salt bridges in GlacPETase: evident impact on its stability and PET catalytic activity

Salt bridges play an important role in the thermostability and function of many enzymes (15). In this study, alanine single mutation in GlacPETase was used to validate the roles of these unique salt bridges in its thermostability and PET hydrolytic activity. These alanine mutants were individually expressed and purified. Then, the mutated proteins underwent melting temperature (Tm) evaluation and PET activity analysis. Results showed that compared to the WT, the Tm of R271A, E275A, D229A, R238A, K78A, E79A, K115A, D159A, E282A, E124A, and R127A have decreased. The Tm value of E282A showed the greatest reduction, 8°C below that of the WT. Next, the Tm values of R271A and D229A decreased by 5°C each. The Tm of R280A remained unchanged, whereas E86A exhibited an increment of 2°C, and both R53A and E111A increased by 1°C (Fig. 4A). The Tm value difference between the two single mutants forming every salt bridge was less than 2°C, except for the difference between R280A and E282A, which reached 8°C. In terms of PET hydrolytic activity, only E111A displayed an enhancement, reaching 145.5% of the WT's activity. By contrast, the activities of all other mutants were reduced by varying degrees (Fig. 4B). Among them, the activities of R271A, E282A, and D229A were only 17.5%, 21.8%, and 28.5% of the WT, respectively.

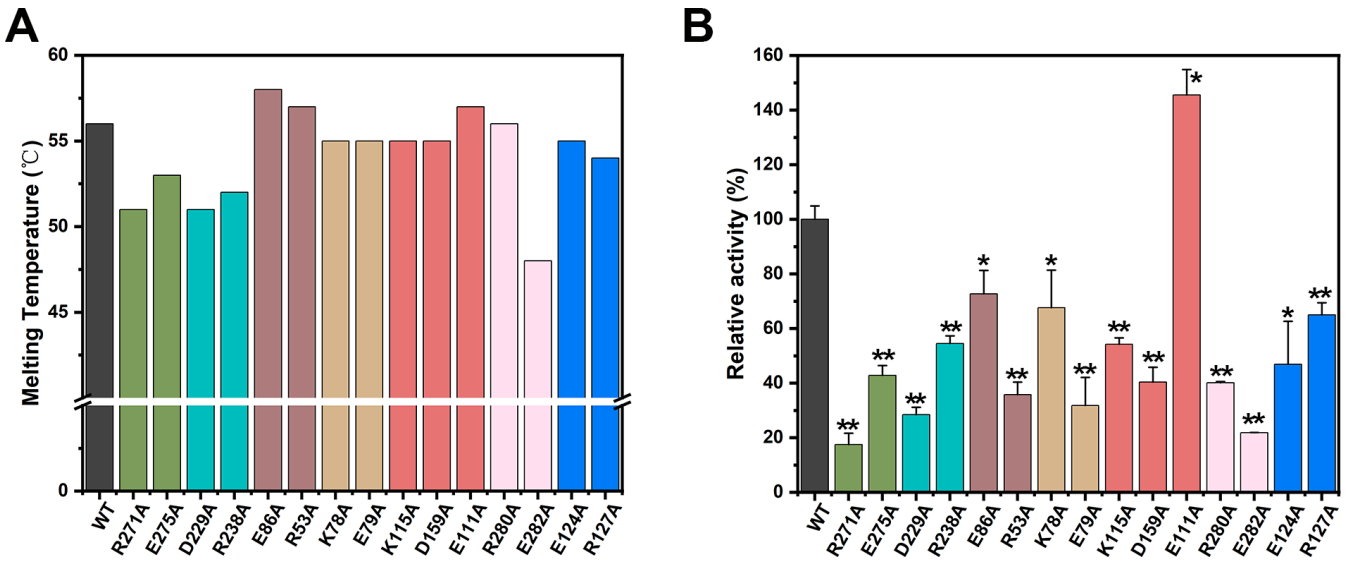

FIG 4 The melting temperature and PET hydrolysis activity of GlacPETase and its mutants associated with salt bridges. (A) The melting temperature of GlacPETase and its mutants. (B) The relative activities of GlacPETase and its mutants. The asterisks (* and **) indicate significant ($P < 0.05$ and $P < 0.01$, respectively) differences between salt bridge mutants and wild type.

MD simulations unveil the stabilizing roles of salt bridges in GlacPETase

Molecular Dynamics (MD) simulation was used to obtain atomistic insights into the mechanism of salt bridge roles. Figure 5 displays the average RMSF for Cα of residues surrounding each pair of salt bridges in WT and the aforementioned single-point alanine mutants. As shown in Fig. 5A through C, the RMSF of adjacent residues within the three pairs of salt bridges, namely R280/E282, R271/E275, and D229/R238, exhibited most notable variations compared to the WT. However, the variations of RMSF were minor in other salt bridge mutants (Fig. 5D through G). This observation was consistent with the changes in the protein melting temperatures, indicating that the three pairs of salt bridges R280/E282, R271/E275, and D229/R238 exerted a more substantial impact on the thermostability of GlacPETase compared with the other salt bridges. The disruption of the D229/R238 salt bridge led to obvious fluctuations in the loop between D229 and R238 during the molecular dynamics simulations. Similarly, the mutation of the R271/E275 salt bridge resulted in more fluctuations in the α-helix (residues 267–275) where the salt bridge was located, as well as the subsequent loop (residues 276–279). The disruption of the R280/E282 salt bridge led to more fluctuations in the preceding loop (residues 276–279) of the β-sheet where the salt bridge was located, as well as the latter half of the connected α-helix (residues 271–275). These findings provided evidence for the stabilizing roles of these salt bridges in their surrounding structures.

Conserved distribution of disulfide bonds and salt bridges in GlacPETase-like proteins

To investigate the phylogenetic relationships among PET hydrolases, a phylogenetic tree was constructed for 68 identified PET hydrolases and their 632 homologous proteins. It was evident that the identified PET hydrolases (marked with red color in Fig. 6A) were distributed diversely across the entire tree, forming two main clades and several smaller branches. GlacPETase was classified into a distinct branch (Fig. 6A), and its closely related homologs exhibited similar distributions of the disulfide bonds and salt bridges (Fig. 6B). The two cysteines involved in disulfide bond formation in GlacPETase were conserved in all nearby homologous proteins except in WP 199286989.1, where only one of cysteine was identified. Regarding salt bridges, the following three pairs were strictly conserved: D196/H227, E124/R127, and K78/E79. At positions E275, E86, and E282, glutamic acid was

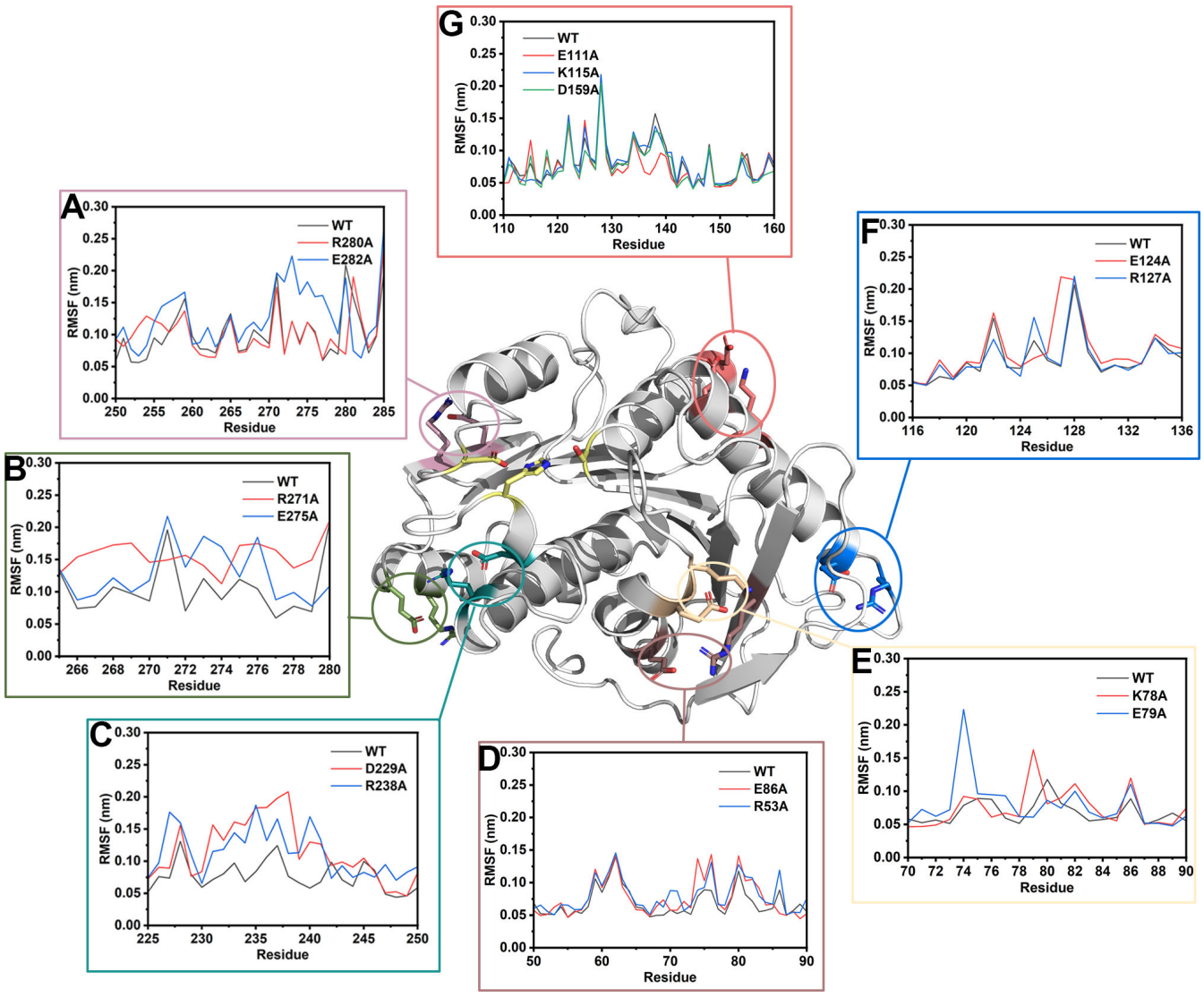

FIG 5 Molecular dynamics simulations analysis of GlacPETase and salt bridge mutants. The average RMSF for Cα of residues surrounding each pair of salt bridges were marked with boxes and circles of the same color (A–G).

substituted by the similarly negatively charged aspartic acid. At position D159, aspartic acid was replaced by the similarly negatively charged glutamic acid. At positions R238 and R271, arginine was replaced by similar amino acids such as glutamine or glutamic acid.

DISCUSSION

In the present study, we determined the crystal structure of GlacPETase using X-ray crystallography. Structural analysis revealed that GlacPETase formed a disulfide bond at the N-terminus and harbored a unique salt bridge network. Site-directed mutagenesis experiments demonstrated that the disulfide bond did not impact GlacPETase's thermostability or catalytic activity toward PET but some salt bridges did affect these properties. Furthermore, molecular dynamics simulations provided insights into the dynamic salt bridge network and their roles in preserving the structural stability of GlacPETase.

In previous studies, disulfide bonds were considered to play an important role in the thermostability and enzymatic activity of PET hydrolases (9, 16, 17). Disrupting the

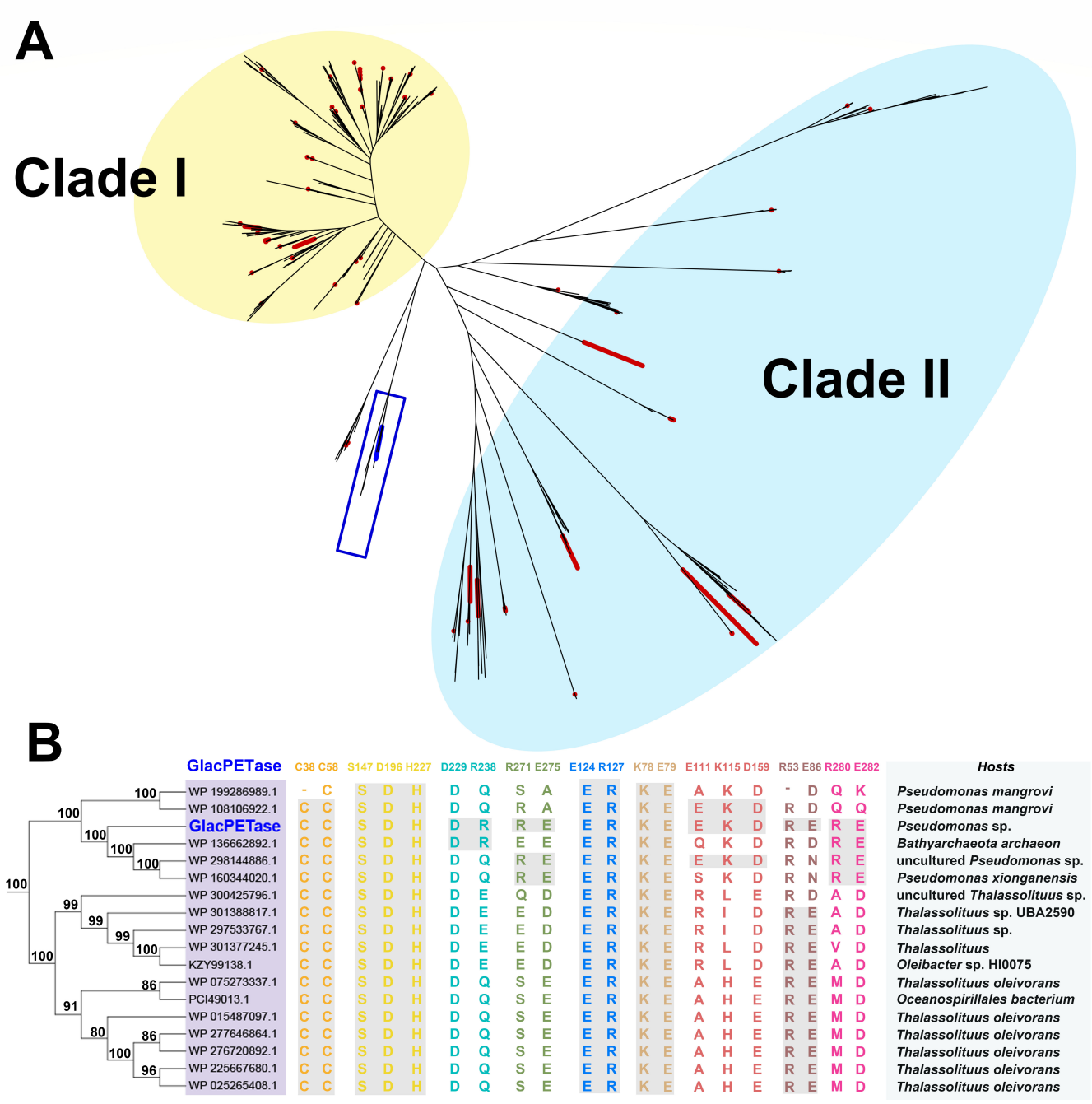

FIG 6 Phylogenetic analysis of PET hydrolase-like proteins. (A) The phylogenetic tree of 68 identified PET hydrolases and their homologs. The identified PET hydrolases were marked with red color and GlacPETase was marked with blue color. Boxed sequences were shown in panel B. (B) The distribution of residues involved in disulfide bonds and salt bridges in homologs within the same branch of GlacPETase. The disulfide bonds and salt bridges conserved strictly in homologs were colored with a gray background. The hosts of these homologs were also displayed.

disulfide bond near the active site in *Is*PETase resulted in a reduction of the melting temperature by approximately 13°C, accompanied by a sharp decline in its PET hydrolytic activity (9). Similarly, disrupting the disulfide bond at the C-terminus in LCC resulted in a reduction of approximately 15°C in its melting temperature (16). In addition, Huang et al. employed two computational algorithms to rationally introduce an additional disulfide bond into *Bb*PETase, resulting in an increase of nearly 15°C in its melting temperature (18). It was reported that the introduction of two disulfide bonds into *Ca*PETase by

rational design resulted in an increment in its melting temperature by nearly 9°C (19). Surprisingly, the disruption of the N-terminal disulfide bond of GlacPETase in this study did not adversely affect both its thermostability and PET hydrolytic activity. As shown in Fig. 1C, the N-terminal disulfide bond of GlacPETase connects the loop preceding β1 and β2. It was reported that the interactions between two β-sheets typically involve hydrogen bonds, Van der Waals forces, and hydrophobic interactions, maintaining a certain level of rigidity in the protein structure (20). In GlacPETase, these interactions naturally exist between β2 preceding C58 and β1 containing C38 (Fig. 1C), maintaining the structural stability in this vicinity. Therefore, disrupting this disulfide bond did not significantly impact the neighboring structure. This unexpected result seems to challenge conventional assumptions about the role of disulfide bonds in PET hydrolases, suggesting a more intricate interplay of factors governing the entire stability of PET hydrolase.

Salt bridges have been demonstrated in previous studies to play a crucial role in maintaining protein stability by enhancing the rigidity of the protein structure (21–24). Furthermore, the introduction of salt bridges has been proven to enhance the thermostability of PET hydrolases (12, 25, 26). In this study, the distribution of salt bridges in major PET hydrolases was systematically analyzed (Table 1), demonstrating the presence of a distinctive salt bridge network in GlacPETase. Site-directed mutagenesis experiments showed that the majority of the salt bridge mutants exhibited a reduction in their melting temperatures, indicating a reduced thermostability. It is noteworthy that the difference in the decrease in melting temperatures caused by the two mutants in the same salt bridge was generally within 2°C, suggesting that the disruption of salt bridges was the primary factor contributing to the reduction in melting temperatures. However, for the same salt bridge, E282A exhibited an 8°C lower melting temperature compared to R280A. From the results of molecular dynamics simulations, the residues 266 to 280 in the E282A mutant displayed more significant fluctuations compared to the WT and R280A counterparts (Fig. 5A), suggesting additional roles of E282 from forming of a salt bridge with R280. An analogous case also occurred in the engineering of *Is*PETase, where a new salt bridge formed between I168R and D186 after the I168R mutation and the guanidine group of I168R also established new hydrogen bonding interactions with the amide oxygen and backbone oxygen atoms of S188Q (26). It was reported that PET hydrolytic activities of PET hydrolases are correlated with enzyme stability (10). In this study, the reduced stability by salt bridge disruption may well led to the enzymes exerting their activity for a shorter duration at the same test temperature, resulting in relatively lower total hydrolysis product yields. Moreover, it is possible that these salt bridge sites are also involved in binding the PET substrate, resulting in reduced activity after mutations. Nevertheless, validating this hypothesis certainly requires obtaining co-crystal structures of PET with different mutants.

A noteworthy mutation was E111A, which exhibited increased thermostability and PET hydrolytic activity after alanine mutation (Fig. 4). This might be attributed to the elimination of electrostatic repulsion between E111 and D159, as E111 was located opposite to D159 (Fig. 3G). The salt bridge between D159 and K115 stabilizes the positions of the two helices (α2 and α3). After the alanine mutation, the electrostatic repulsion ceased, leading to enhanced thermostability. However, the increased PET hydrolytic activity of E111A cannot be solely attributed to its improved thermostability. Other factors such as a more favorable substrate binding might contribute, which needs further explanation through the determination of complex structures.

Compared with its homologs, GlacPETase exhibits moderate thermostability (Table 2). The stronger thermostability of GlacPETase compared to *Is*PETase may be attributed to the stabilizing contribution of salt bridges in GlacPETase, outweighing the stability supported by disulfide bonds and other factors in *Is*PETase. The lower thermostability of GlacPETase compared to TfH, TfCut2, and LCC may be due to the greater contribution of disulfide bonds or other factors in these proteins. The contribution of each influencing

TABLE 2 Comparison in the melting temperature of GlacPETase and some representative PET hydrolases[a]

	Protein	Melting temperature (°C)	Reference
Wild Type	GlacPETase	56	(13)
	*Is*PETase	49	(13)
	TfH	70	(27)
	TfCut2	68	(9)
	LCC	86	(16)
Disruption of disulfide bonds	GlacPETase^{C38S}	T_m^{WT}+2	This study
	GlacPETase^{C58S}	T_m^{WT}+2	This study
	*Is*PETase$^{C203A/C239A}$	T_m^{WT}-13	(9)
	LCC^{C292A}	T_m^{WT}-15	(16)
Disruption of salt bridges	GlacPETase^{R271A}	T_m^{WT}-8 ~T_m^{WT}-1	This study
	GlacPETase^{E275A}		
	GlacPETase^{D229A}		
	GlacPETase^{R238A}		
	GlacPETase^{K78A}		
	GlacPETase^{E79A}		
	GlacPETase^{K115A}		
	GlacPETase^{D159A}		
	GlacPETase^{E282A}		
	GlacPETase^{E124A}		
	GlacPETase ^{R127A}		
Build of salt bridges	*Is*PETase$^{I168R/S188D}$	T_m^{WT}+7	(12)
	*Is*PETase$^{I168R/S188E}$	T_m^{WT}+8	(12)

[a]The measured melting temperatures may vary due to different experimental conditions employed by different experimenters, but the overall difference does not exceed 5°C. T_m^{WT} refers to the melting temperature of the wild type under the same experimental conditions as the mutants.

factor may be related to their respective positions and the strength of the interactions, which requires further experimental analysis.

In 2018, Joo et al. classified PET hydrolase-like enzymes into two types based on their sequence and structural information (9). Type I PET hydrolases possess a single conserved disulfide bond at the C-terminus. Type II PET hydrolases feature an additional disulfide bond and an extended loop near the catalytic triad in addition to the C-terminal disulfide bond in Type I PET hydrolases (9). However, with the continuous discovery of new PET hydrolases in recent years, this classification criterion seems to be inadequate. For instance, GlacPETase in this study has a unique N-terminal disulfide bond and a unique salt bridge network, making it apart from Type I and Type II PET hydrolases. Another case is FsC, which displays significant structural differences from both Type I and Type II PET hydrolases, despite also being an α/β hydrolase. In addition, some PET hydrolases exhibited some significant modifications in the core fold and some PET hydrolases possessed extra structural domains (28). In this study, the phylogenetic analysis of identified PET hydrolases and their homologs further reflected the diversity of PET hydrolases (Fig. 6). Therefore, when classifying PET hydrolases, other structural features such as salt bridges, domains, overall structural similarities, and additional factors are also suggested to be considered.

Notably, most of the hosts harboring GlacPETase-like enzymes belong to the Pseudomonadota Phylum, such as *Pseudomonas mangrovi*, *Thalassolittus,* and *Oceanospirillales* (Fig. 6B). This observation underscores their evolutionary resemblance, suggesting a shared evolutionary trajectory among these enzymes. Strains in the same genus as these hosts are often reported to be associated with the degradation of hydrocarbons such as petroleum and alkanes (29). Therefore, these enzymes may have evolved from enzymes with the function of degrading hydrocarbons in these strains to enable the utilization of PET as a carbon source for growth.

In conclusion, the structural analysis of GlacPETase derived from glacial microbiomes revealed its unique salt bridge network crucial for its stability, marking it as a promising

candidate for further protein engineering. These discoveries contribute significantly to our fundamental knowledge of the thermostability in PET hydrolases but also underscore the immense diversity and adaptability within this enzyme family, offering hope for addressing the global plastic pollution crisis.

MATERIALS AND METHODS

Protein expression and purification

The expression and purification of GlacPETase were carried out as previously reported (13). Briefly, the gene *GlacPETase* was cloned into the pET-32a vector using *Eco*RI (5′ end) and *Not*I (3′ end) sites, fused to the N-terminal TrxA-coding sequence. A TEV protease recognition site was introduced between *trxA* and *glacPETase*. The resulting plasmid was transformed into *E. coli* BL21 trxB (DE3), cultured in LB with 100 µg/mL ampicillin at 20°C for 48 h. After the harvest by centrifugation and lysed by ultrasonication, the supernatant underwent Ni-NTA chromatography for purification. Following TrxA-tag removal through TEV protease digestion and additional Ni-NTA chromatography, the mature GlacPETase was obtained. Then, the GlacPETase for crystallization was further purified using a gel filtration chromatography column (GE Healthcare Life Sciences, Boston, MA) in buffer (20 mM Tris-HCl, pH 8, 300 mM NaCl). Then, the protein was ultrafiltered to 11 mg/mL for crystallization screening.

Crystallization, data collection and structure refinement

Crystallization of the purified GlacPETase was performed using the sitting-drop vapor-diffusion method at 20°C. Each experiment consisted of 0.5 µL or 1 µL of GlacPETase (11 mg/mL) containing solution (20 mM Tris-HCl, 300 mM NaCl, pH 8.0) and 0.5 µL of reservoir solution. Then it was equilibrated against 50 µL of the reservoir solution. Diffraction-quality crystals of GlacPETase appeared within 3 days. The best quality GlacPETase crystals were grown in 0.1 M Tris, 0.1 M potassium thiocyanate, 0.1 M sodium bromide, and 25% vol/vol PEG smear Broad (pH 7.8). For data collection, the aforementioned crystals were flash-frozen by immersion in liquid nitrogen after being bathed in a reservoir solution containing 20% glycerol as a cryoprotectant. Data were gathered at 100 K at the Shanghai Synchrotron Radiation Facility (BL19U beamline) and then were integrated, scaled, and merged by HKL3000 (30). Phaser in the CCP4 program suite (31) was used to carry out the molecular replacement, and the structure of GlacPETase predicted by AlphaFold2 (32) was set as the template. The structure was manually adjusted using COOT (33) and then refined using Phenix (34).

Evaluation of salt bridges in GlacPETase and their ASA analysis

Salt bridges in GlacPETase were analyzed using "Salt Bridges and charge segregation" in ProteinTools (35). GetArea was used to compute the Solvent ASA of residues involved in salt bridges (36), which was then converted to %ASA as reported (23).

Site-directed mutagenesis

Site-directed mutagenesis experiments were conducted using a Site-Directed Mutagenesis Kit (Hieff Mut, Yeasen Biotechnology Co., Ltd., Shanghai, China). Mutagenic primers are provided in supplementary materials (Table S1). The expression and purification of mutants of GlacPETase were the same as described above.

Enzyme activity and melting temperature (Tm) measurement

The activity of wild type and mutants of GlacPETase was determined using PET nanoplastics as substrates. The assay was carried out as a previously reported method with some modifications (13). Briefly, 1 mL of 500 nM protein was incubated with 10 µL of 1% PET stock solutions at 30°C for 24 h. The reaction process was terminated

by adding 1 mL of acetonitrile and the supernatant was centrifuged and filtered for high-performance liquid chromatography analysis. The profile for HPLC analysis was the same as reported previously (13). The relative enzyme activity of mutants was assessed by calculating the ratio of the total hydrolysis products (BHET, MHET, and TPA) to that of the wild type. The melting temperatures of wild type and mutants were performed using the Thermofluor assay as reported previously (13). Three replicates were conducted for each mutant and the wild type in both thermostability and enzymatic activity tests. *T*-test was used to validate whether there is a significant difference between mutants and wild type.

Phylogenetic analysis and multiple sequence alignment

To obtain homologous proteins of PET hydrolases, 68 identified PET hydrolases were utilized as query sequences in BLASTp searches against the Non-Redundant Protein Sequence Database (37). The amino acid sequences of these 68 known PET hydrolases were placed into Text S1 in supplementary materials. The search was carried out using DIAMOND (v0.9.25.126) employing an e-value threshold of $1e^{-5}$ and requiring a minimum identity and coverage of 30% (38). After removing redundancy, a total of 632 sequences were obtained. These sequences, along with the initial set of 68 identified PET hydrolases, were further aligned using MAFFT-linsi (version 7) with the FFT-NS-2 algorithm (39). Then, a phylogenetic tree of these PET hydrolase-like proteins was constructed using IQ-TREE (version 2.2.2.6) (40) with the "WAG + F + I + G4" model and 1,000 ultrafast bootstraps. The Plastics-Active Enzymes Database presented an overview of the accessions corresponding to the 68 PET hydrolases examined in this research (41). Then, three thermophilic PET hydrolases (LCC, Cut190, and TfCut_2) and three mesophilic PET hydrolases (*Is*PETase, PE-H, and Ple629) were subjected to multiple sequence alignment with GlacPETase using MAFFT-linsi (version 7) (39), shown by ESPript (version 3.0) (42).

Molecular dynamics simulations

GROMACS 2021 with the AMBER99SB force field was used to perform molecular dynamics simulations (43). Proteins were immersed in a TIP3P water box with octahedral boundaries. The system's unbalanced charge was neutralized by supplementing with appropriate counterions (sodium ions and chloride ions). The system underwent energy minimization by the steepest descent algorithm, followed by 100 ps of equilibration in the *NVT* and *NPT* ensembles. A force constant of 1,000 KJ mol^{-1} nm^{-1} was used to restrain all heavy atoms. Unrestrained production runs were performed for 20 ns in the *NPT* ensemble at 340 K (66°C), with a 2 fs time step.

ACKNOWLEDGMENTS

This study was supported by the National Key Research and Development Program of China [grant 2021YFC2103600] and the Seed Industry Revitalization Project of Guangdong Province [grant 23050202].

AUTHOR AFFILIATIONS

[1]State Key Laboratory of Microbial Metabolism, Joint International Research Laboratory of Metabolic and Developmental Sciences, and School of Life Sciences and Biotechnology, Shanghai Jiao Tong University, Shanghai, China
[2]Center for Pan-third Pole Environment, Lanzhou University, Lanzhou, China

AUTHOR ORCIDs

Xiaoyan Qi http://orcid.org/0000-0001-8599-139X
Chao-Fan Yin http://orcid.org/0000-0002-6905-0909
Ying Xu http://orcid.org/0000-0001-5936-0818

Ning-Yi Zhou http://orcid.org/0000-0002-0917-5750

FUNDING

Funder	Grant(s)	Author(s)
MOST | National Key Research and Development Program of China (NKPs)	2021YFC2103600	Ying Xu
The seed industry Revitalization Project of Guangdong Province	23050202	Ning-Yi Zhou

DATA AVAILABILITY

The diffraction data and the protein structure of GlacPETase have been uploaded to the Protein Data Bank (accession number 8X6V).

ADDITIONAL FILES

The following material is available online.

Supplemental Material

Tables S1 to S3, Fig. S1, Text S1 (AEM02242-23-s0001.docx). Supplemental material.

REFERENCES

1. PlasticsEurope. 2021. Plastics – the facts 2021: an analysis of European plastics production, demand and waste data
2. Geyer R, Jambeck JR, Law KL. 2017. Production, use, and fate of all plastics ever made. Sci Adv 3:e1700782. https://doi.org/10.1126/sciadv.1700782
3. Andrady AL. 2022. Weathering and fragmentation of plastic debris in the ocean environment. Mar Pollut Bull 180:113761. https://doi.org/10.1016/j.marpolbul.2022.113761
4. Wu P, Huang J, Zheng Y, Yang Y, Zhang Y, He F, Chen H, Quan G, Yan J, Li T, Gao B. 2019. Environmental occurrences, fate, and impacts of microplastics. Ecotoxicol Environ Saf 184:109612. https://doi.org/10.1016/j.ecoenv.2019.109612
5. Kawai F, Kawabata T, Oda M. 2020. Current state and perspectives related to the polyethylene terephthalate hydrolases available for biorecycling. ACS Sustainable Chem Eng 8:8894–8908. https://doi.org/10.1021/acssuschemeng.0c01638
6. Chae Y, An YJ. 2018. Current research trends on plastic pollution and ecological impacts on the soil ecosystem: a review. Environ Pollut 240:387–395. https://doi.org/10.1016/j.envpol.2018.05.008
7. Kawai F, Kawabata T, Oda M. 2019. Current knowledge on enzymatic PET degradation and its possible application to waste stream management and other fields. Appl Microbiol Biotechnol 103:4253–4268. https://doi.org/10.1007/s00253-019-09717-y
8. Yoshida S, Hiraga K, Takehana T, Taniguchi I, Yamaji H, Maeda Y, Toyohara K, Miyamoto K, Kimura Y, Oda K. 2016. A bacterium that degrades and assimilates poly(ethylene terephthalate). Science 351:1196–1199. https://doi.org/10.1126/science.aad6359
9. Joo S, Cho IJ, Seo H, Son HF, Sagong HY, Shin TJ, Choi SY, Lee SY, Kim KJ. 2018. Structural insight into molecular mechanism of poly(ethylene terephthalate) degradation. Nat Commun 9:382. https://doi.org/10.1038/s41467-018-02881-1
10. Ronkvist ÅM, Xie W, Lu W, Gross RA. 2009. Cutinase-catalyzed hydrolysis of poly(ethylene terephthalate). Macromolecules 42:5128–5138. https://doi.org/10.1021/ma9005318
11. Tournier V, Topham CM, Gilles A, David B, Folgoas C, Moya-Leclair E, Kamionka E, Desrousseaux M-L, Texier H, Gavalda S, Cot M, Guémard E, Dalibey M, Nomme J, Cioci G, Barbe S, Chateau M, André I, Duquesne S, Marty A. 2020. An engineered PET depolymerase to break down and recycle plastic bottles. Nature 580:216–219. https://doi.org/10.1038/s41586-020-2149-4
12. Qu Z, Chen K, Zhang L, Sun Y. 2023. Computation-based design of salt bridges in PETase for enhanced thermostability and performance for PET degradation. Chembiochem 24:e202300373. https://doi.org/10.1002/cbic.202300373
13. Qi X, Ji M, Yin CF, Zhou NY, Liu Y. 2023. Glacier as a source of novel polyethylene terephthalate hydrolases. Environ Microbiol 25:2822–2833. https://doi.org/10.1111/1462-2920.16516
14. Han X, Liu WD, Huang JW, Ma JT, Zheng YY, Ko TP, Xu LM, Cheng YS, Chen CC, Guo RT. 2017. Structural insight into catalytic mechanism of PET hydrolase. Nat Commun 8:2106. https://doi.org/10.1038/s41467-017-02255-z
15. Elcock AH. 1998. The stability of salt bridges at high temperatures: implications for hyperthermophilic proteins. J Mol Biol 284:489–502. https://doi.org/10.1006/jmbi.1998.2159
16. Sulaiman S, You DJ, Kanaya E, Koga Y, Kanaya S. 2014. Crystal structure and thermodynamic and kinetic stability of metagenome-derived LC-cutinase. Biochemistry 53:1858–1869. https://doi.org/10.1021/bi401561p
17. Liu B, He L, Wang L, Li T, Li C, Liu H, Luo Y, Bao R. 2018. Protein crystallography and site-direct mutagenesis analysis of the poly(ethylene terephthalate) hydrolase PETase from *Ideonella sakaiensis*. Chembiochem 19:1471–1475. https://doi.org/10.1002/cbic.201800097
18. Huang D, Zhang L, Sun Y. 2023. Rational design of disulfide bridges in BbPETase(CD) for enhancing the enzymatic performance in PET degradation. Molecules 28:3528. https://doi.org/10.3390/molecules28083528
19. Hong HS, Ki D, Seo H, Park J, Jang J, Kim KJ. 2023. Discovery and rational engineering of PET hydrolase with both mesophilic and thermophilic PET hydrolase properties. Nat Commun 14:4556. https://doi.org/10.1038/s41467-023-40233-w
20. Cohen N, Eisenbach CD. 2020. Molecular mechanics of beta-sheets. ACS Biomater Sci Eng 6:1940–1949. https://doi.org/10.1021/acsbiomaterials.9b01983
21. Szilágyi A, Závodszky P. 2000. Structural differences between mesophilic, moderately thermophilic and extremely thermophilic protein subunits: results of a comprehensive survey. Structure 8:493–504. https://doi.org/10.1016/s0969-2126(00)00133-7
22. Makhatadze GI, Loladze VV, Ermolenko DN, Chen X, Thomas ST. 2003. Contribution of surface salt bridges to protein stability: guidelines for protein engineering. J Mol Biol 327:1135–1148. https://doi.org/10.1016/s0022-2836(03)00233-x
23. Kaira GS, Usharani D, Kapoor M. 2019. Salt bridges are pivotal for the kinetic stability of GH26 endo-mannanase (ManB-1601). Int J Biol

Macromol 133:1236–1241. https://doi.org/10.1016/j.ijbiomac.2019.04.175
24. Zhang R, He L, Shen J, Miao Y, Tang X, Wu Q, Zhou J, Huang Z. 2020. Improving low-temperature activity and thermostability of exo-inulinase InuAGN25 on the basis of increasing rigidity of the terminus and flexibility of the catalytic domain. Bioengineered 11:1233–1244. https://doi.org/10.1080/21655979.2020.1837476
25. Yin Q, You S, Zhang J, Qi W, Su R. 2022. Enhancement of the polyethylene terephthalate and mono-(2-hydroxyethyl) terephthalate degradation activity of *Ideonella sakaiensis* PETase by an electrostatic interaction-based strategy. Bioresour Technol 364:128026. https://doi.org/10.1016/j.biortech.2022.128026
26. Cui YL, Chen YC, Liu XY, Dong SJ, Tian YE, Qiao YX, Mitra R, Han J, Li CL, Han X, Liu WD, Chen Q, Wei WQ, Wang X, Du WB, Tang SY, Xiang H, Liu HY, Liang Y, Houk KN, Wu B. 2021. Computational redesign of a PETase for plastic biodegradation under ambient condition by the GRAPE strategy. ACS Catal 11:1340–1350. https://doi.org/10.1021/acscatal.0c05126
27. Then J, Wei R, Oeser T, Barth M, Belisário-Ferrari MR, Schmidt J, Zimmermann W. 2015. Ca2+ and Mg2+ binding site engineering increases the degradation of polyethylene terephthalate films by polyester hydrolases from *Thermobifida fusca*. Biotechnol J 10:592–598. https://doi.org/10.1002/biot.201400620
28. Erickson E, Gado JE, Avilán L, Bratti F, Brizendine RK, Cox PA, Gill R, Graham R, Kim D-J, König G, Michener WE, Poudel S, Ramirez KJ, Shakespeare TJ, Zahn M, Boyd ES, Payne CM, DuBois JL, Pickford AR, Beckham GT, McGeehan JE. 2022. Sourcing thermotolerant poly(ethylene terephthalate) hydrolase scaffolds from natural diversity. Nat Commun 13:7850. https://doi.org/10.1038/s41467-022-35237-x
29. Teramoto M, Ohuchi M, Hatmanti A, Darmayati Y, Widyastuti Y, Harayama S, Fukunaga Y. 2011. *Oleibacter marinus* gen. nov., sp. nov., a bacterium that degrades petroleum aliphatic hydrocarbons in a tropical marine environment. Int J Syst Evol Microbiol 61:375–380. https://doi.org/10.1099/ijs.0.018671-0
30. Minor W, Cymborowski M, Otwinowski Z, Chruszcz M. 2006. HKL-3000: the integration of data reduction and structure solution--from diffraction images to an initial model in minutes. Acta Crystallogr D Biol Crystallogr 62:859–866. https://doi.org/10.1107/S0907444906019949
31. BaileyS1994. The Ccp4 suite: Programs for protein crystallography. Acta Crystallogr D Biol Crystallogr 50:760–763. https://doi.org/10.1107/S0907444994003112
32. Jumper J, Evans R, Pritzel A, Green T, Figurnov M, Ronneberger O, Tunyasuvunakool K, Bates R, Žídek A, Potapenko A, et al. 2021. Highly accurate protein structure prediction with AlphaFold. Nature 596:583–589. https://doi.org/10.1038/s41586-021-03819-2
33. Emsley P, Cowtan K. 2004. Coot: model-building tools for molecular graphics. Acta Crystallogr D Biol Crystallogr 60:2126–2132. https://doi.org/10.1107/S0907444904019158
34. Liebschner D, Afonine PV, Baker ML, Bunkóczi G, Chen VB, Croll TI, Hintze B, Hung LW, Jain S, McCoy AJ, Moriarty NW, Oeffner RD, Poon BK, Prisant MG, Read RJ, Richardson JS, Richardson DC, Sammito MD, Sobolev OV, Stockwell DH, Terwilliger TC, Urzhumtsev AG, Videau LL, Williams CJ, Adams PD. 2019. Macromolecular structure determination using X-rays, neutrons and electrons: recent developments in Phenix. Acta Crystallogr D Struct Biol 75:861–877. https://doi.org/10.1107/S2059798319011471
35. Ferruz N, Schmidt S, Höcker B. 2021. ProteinTools: a toolkit to analyze protein structures. Nucleic Acids Res 49:W559–W566. https://doi.org/10.1093/nar/gkab375
36. Fraczkiewicz R, Braun W. 1998. Exact and efficient analytical calculation of the accessible surface areas and their gradients for macromolecules. J Comput Chem 19:319–333. https://doi.org/10.1002/(SICI)1096-987X(199802)19:3<319::AID-JCC6>3.0.CO;2-W
37. Pruitt KD, Tatusova T, Maglott DR. 2007. NCBI reference sequences (RefSeq): a curated non-redundant sequence database of genomes, transcripts and proteins. Nucleic Acids Res 35:D61–D65. https://doi.org/10.1093/nar/gkl842
38. Morris GM, Huey R, Lindstrom W, Sanner MF, Belew RK, Goodsell DS, Olson AJ. 2009. AutoDock4 and AutoDockTools4: automated docking with selective receptor flexibility. J Comput Chem 30:2785–2791. https://doi.org/10.1002/jcc.21256
39. Katoh K, Misawa K, Kuma K, Miyata T. 2002. MAFFT: a novel method for rapid multiple sequence alignment based on fast fourier transform. Nucleic Acids Res 30:3059–3066. https://doi.org/10.1093/nar/gkf436
40. Minh BQ, Schmidt HA, Chernomor O, Schrempf D, Woodhams MD, von Haeseler A, Lanfear R. 2020. IQ-TREE 2: new models and efficient methods for phylogenetic inference in the genomic era. Mol Biol Evol 37:1530–1534. https://doi.org/10.1093/molbev/msaa015
41. Buchholz PCF, Feuerriegel G, Zhang H, Perez-Garcia P, Nover LL, Chow J, Streit WR, Pleiss J. 2022. Plastics degradation by hydrolytic enzymes: the plastics-active enzymes database-PAZy. Proteins 90:1443–1456. https://doi.org/10.1002/prot.26325
42. Robert X, Gouet P. 2014. Deciphering key features in protein structures with the new ENDscript server. Nucleic Acids Res 42:W320–W324. https://doi.org/10.1093/nar/gku316
43. Hornak V, Abel R, Okur A, Strockbine B, Roitberg A, Simmerling C. 2006. Comparison of multiple Amber force fields and development of improved protein backbone parameters. Proteins 65:712–725. https://doi.org/10.1002/prot.21123